

# Electromagnetic Waves from TNT Explosions

A. L. Kuhl, D. A. White, B. A. Kirkendall

Lawrence Livermore National Laboratory, Livermore, California, USA  
Email: [kuhl2@llnl.gov](mailto:kuhl2@llnl.gov)

Received 29 May 2014; revised 25 June 2014; accepted 21 July 2014

Copyright © 2014 by authors and Scientific Research Publishing Inc.  
This work is licensed under the Creative Commons Attribution International License (CC BY).  
<http://creativecommons.org/licenses/by/4.0/>



Open Access

---

## Abstract

Experimental observations indicate that electromagnetic (EM) radiation is emitted after the detonation of high explosives (HE) charges. The movement of ionized atoms, particles and electrons seems to be the underlying cause. Expansion of the detonation products (DP) drives a strong (~1 kb) shock in surrounding air. This forms an intense thermal wave ( $T \sim 11,000$  K) with duration of ~20 microseconds. Such temperatures create significant ionization of the air. According to Ohm's Law, movement of ionized patches generates current; and according to the Biot-Savart Law, such currents induce electric and magnetic fields. We investigate these effects through numerical simulations of TNT explosions. A high-order Godunov scheme is used to integrate the one-dimensional conservation laws of gasdynamics. An extremely fine grid (10 microns) was needed to get converged temperature and conductivity profiles. The gasdynamic solution provided a source current, which was fed into a time-domain Green's function code to predict three-dimensional electromagnetic waves emanating from the TNT explosion. This analysis clearly demonstrates one mechanism—the Boronin current—as the source of EM emissions from TNT explosions, but other mechanisms are also possible.

## Keywords

TNT Detonation, Boronin Current, EM Waves, Time-Domain Green's Function

---

## 1. Introduction

In 1954 Kolsky published an article in *Nature* [1] on measurements of electromagnetic (EM) waves emitted from the detonation of high-explosives charges. He used 1-g charges of: PETN, lead azide, silver acetylide and nitrogen tri-iodide. EM waves were measured by a 10-cm-long wire probe connected to wide-band amplifier; the signal was recorded on an oscilloscope. In all cases the probe measured a maximum potential at ~50  $\mu$ s. In 1956 Takakura [2] reported measurements of radio noise generated by the detonation of 0.2-gram lead azide

charges. Signals peaked 80 - 160  $\mu\text{s}$  after detonation. In Cook's book: *The Science of High Explosives* [3] published in 1958, he devoted all of Chapter 7 to the subjects of ionization, electrical, magnetic and electromagnetic phenomena accompanying detonations. In 1990 Boronin *et al.* published a review article [4] on the physical mechanisms of EM field generation created by the detonation of condensed explosive charges. They proposed that "the mechanism for radio radiation generation by an explosion...is associated with the process of acceleration or retardation of certain electron groups in an ionized air layer on the shock front". Here we call this the "*Boronin Effect*". In 2004 Adushkin and Soloviev studied the generation of electric and magnetic fields from above ground, surface and underground explosions [5]; Academician Adushkin concluded that the actual mechanism of RF generation was not known.

Conductivity histories were measured in explosion clouds in a shock tube by Kuhl, Reichenbach and Neuwald [6]. Results are depicted in the time-distance diagram of the combustion cloud (**Figure 1(a)**), showing a shock front followed by a detonation products (DP) cloud. **Figure 1(b)** presents the conductivity history measured at  $x = 1236 \text{ mm}$ . The conductivity pulse begins with the arrival of the DP cloud ( $t = 2.5 \text{ ms}$ ) and decays to zero at  $\sim 6.5 \text{ ms}$  due to charge recombination. The shock reflects off the end wall and passes back through the DP cloud. The reflected shock re-heats and re-ionizes the DP cloud leading to a second conductivity pulse at around 7 ms. The DP cloud is turbulent, which causes turbulent fluctuations in the conductivity pulse. Photodiode measurements of **Figure 1(b)** indicate that the optical pulse (blue curve) coincides with the conductivity pulse (red curve). Thus, when one observes a strong optical output from a fireball, one can be sure that the cloud is conductive.

Here we use the working hypothesis that such EM waves are a result of ionization in explosions. We neglect kinetics effects and assume chemical equilibrium—so ionization is directly coupled to the temperature field<sup>1</sup>. We use our AMR code [7]–[10] to perform high-resolution numerical simulations of explosion fields from 1-kg TNT charges. From the computed velocity and conductivity fields, one can use Ohm's law to construct a current. This current serves as a "source" in a time-domain Green's function code [11], which then predicts the electric and magnetic field histories at various distances from the fireball.

Section §2 describes the properties of high-temperature air, based on thermodynamic equilibrium analysis of Gilmore [12]. Section §3 presents the gas-dynamic conservation laws that govern the explosion field, along with the Equations of State needed to close the system of partial differential equations. The blast wave flow field from a 1-kg TNT charge is presented in Section §4. A model of the EM fields radiated from the TNT cloud is presented in Section §5. This is followed by a discussion of other mechanisms for current generation in Section §6, and conclusions in Section §7.

## 2. Properties of High-Temperature Air

The analysis of high-temperature air is based on the work of Forrest Gilmore [12]. He computed the thermodynamic properties of dry air including: composition, pressure, energy and entropy as a function of temperature and density, over the temperature range:  $1000 \text{ K} < T < 24,000 \text{ K}$  and the density range:  $10^{-6} \leq \rho/\rho_0 \leq 10$ . As defined by Glueckman [13], dry air is composed of the following mole percent species:  $\text{N}_2$  (78.084%),  $\text{O}_2$  (20.946%), A (0.934%),  $\text{CO}_2$  (0.033%), Ne (0.003%); these species form the *Reactants* of the thermodynamic system. Gilmore assumed air to behave as a mixture of ideal gases in chemical equilibrium—including dissociation and ionization effects. The analysis was based on ideal gas internal energies and free energies of 29 different molecules, atoms and ions, forming the following *Products*:

- Monatomic gases:  $\text{e}^-$ , C,  $\text{C}^+$ , N,  $\text{N}^+$ ,  $\text{N}^{++}$ ,  $\text{N}^{+++}$ ,  $\text{O}^-$ , O,  $\text{O}^+$ ,  $\text{O}^{++}$ ,  $\text{O}^{+++}$ , Ne,  $\text{Ne}^+$ , A,  $\text{A}^+$ ,  $\text{A}^{++}$ .
- Diatomic molecules: CO,  $\text{N}_2$ , NO,  $\text{O}_2$  and  $\text{CO}^+$ ,  $\text{N}_2^+$ ,  $\text{NO}^+$ ,  $\text{O}_2^-$ ,  $\text{O}_2^+$ .
- Triatomic molecules:  $\text{CO}_2$ ,  $\text{O}_3$ ,  $\text{NO}_2$ .

Composition of the mixture, as a function of temperature and density, was determined by the "equilibrium constant method", applied to the various chemical reactions. The 29 different composition parameters satisfy 23 different equilibrium equations and 6 conservation equations (for 5 elements plus the conservation of charge). Solution of this set of 29 simultaneous equations was performed by hand, on a desktop calculator<sup>2</sup>.

<sup>1</sup>In the simulations reported here, we assume the gasdynamic approximation: *i.e.*, there are no electric or magnetic forces to influence the momenta of ions and electrons. Therefore, ionization is tied directly to the temperature field.

<sup>2</sup>In modern thermochemical codes such as Cheetah [22], equilibrium states are found by minimizing the Gibbs free energy of the system. This involves inversion of a large matrix, which can be accomplished easily on modern computers. Unfortunately, Cheetah does not take into account ionization effects, so the Gilmore computations [12] were used.

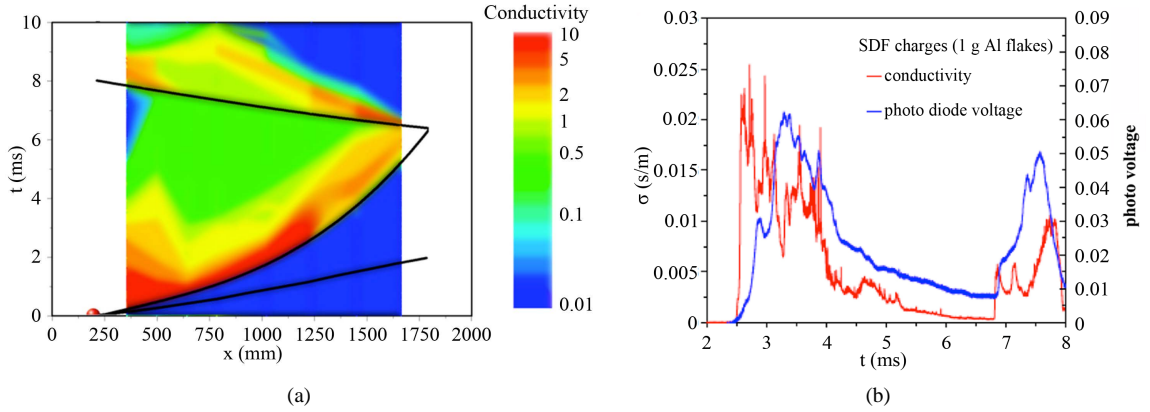


**Figure 1.** Conductivity in an Al-SDF (shock-dispersed-fuel) combustion cloud in a shock tube (Kuhl, 2010). (a) x-t diagram of the shock and combustion cloud; (b) Measured conductivity and luminosity histories.

The locus of thermodynamic states of air from 1000 K to 24,000 K, are presented in the *Le Chatelier* plane of specific internal energy  $E$  versus temperature  $T$  in **Figure 2**. These loci were fit with power law functions:

$$\log(E_i - E_0) = a_i + b_i \cdot (\log T)^{\alpha_i} \quad (1)$$

The fitting constants for different density ratios are given in **Table 1**.

The equilibrium composition of dry air is presented in **Figure 3** for a density ratio  $\rho/\rho_0 = 10$  (corresponding to the strong-shock case studied here). One notes that ionization of nitrous oxide starts at about 4500 K, thereby generating electrons. At higher temperatures atomic nitrogen ionizes and is the main source of electrons, along with ~10% contribution from atomic oxygen.

Electron concentrations from that solution are plotted in **Figure 4** for the same density ratios. These loci are fit with the following functions:

$$\log(C_e) = \begin{cases} 3.35 - 21.0 \cdot \exp[-1.40 \cdot \log(T/1000)] & \text{for } \rho/\rho_0 = 0.1 \\ 2.05 - 22.8 \cdot \exp[-1.71 \cdot \log(T/1000)] & \text{for } \rho/\rho_0 = 1 \\ 1.06 - 25.6 \cdot \exp[-2 \cdot \log(T/1000)] & \text{for } \rho/\rho_0 = 10 \end{cases} \quad (2)$$

which were used to predict electron concentrations in blast wave.

The electrical conductivity of air, covering the temperature range from 6500 K to 11,500 K, was measured by Larson and Williams [14] in a high-pressure (1 - 30 atm.) arc jet facility at AEDC. Experimental results are presented in **Figure 5**. The data points were fit by an exponential function:

$$\sigma = BT^{-C} \exp[-D/T] \quad (3)$$

with  $B = 2.3 \times 10^{12}$  and  $C = 1.8$  and  $D = 8.6 \times 10^{14}$ .

### 3. Gasdynamic Model

#### 3.1. Conservation Laws

We model explosion field by the one-dimensional (1D) conservation laws of gasdynamics [15]:

$$\text{Mass: } \partial_t \rho + \partial_r \rho u = -j \rho u / r \quad (4)$$

$$\text{Momentum: } \partial_t \rho u + \partial_r [\rho u u + p] = -j \rho u^2 / r \quad (5)$$

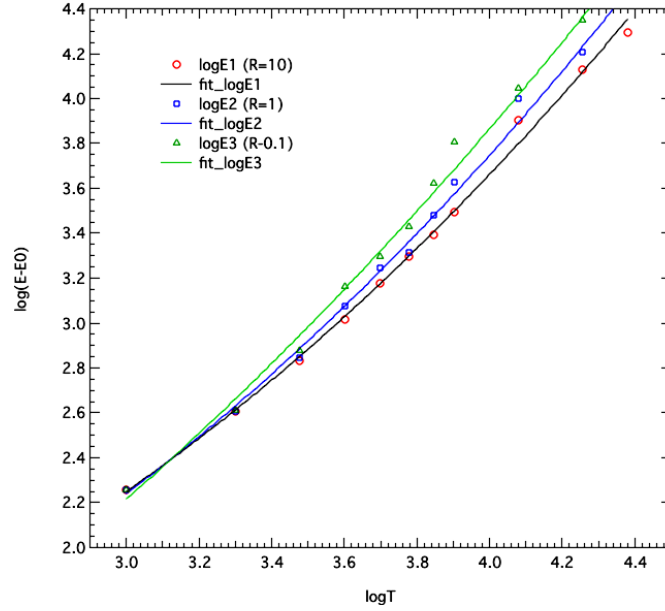
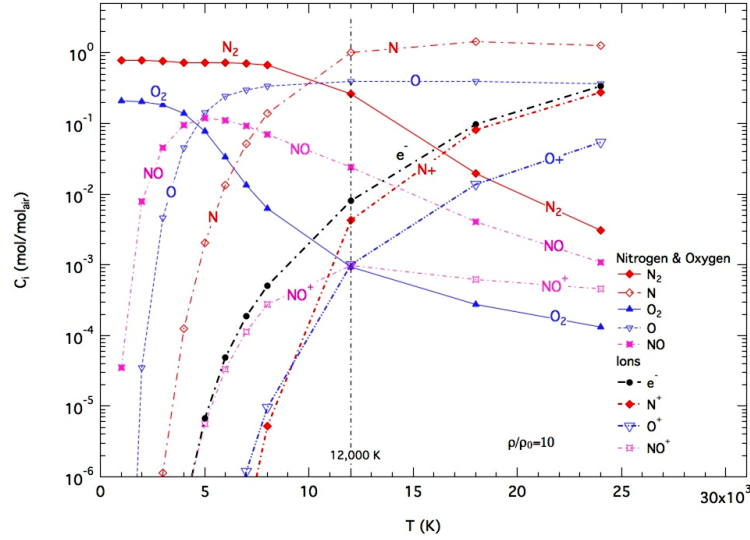
$$\text{Energy: } \partial_t \rho E_T + \partial_r [\rho u E_T + p u] = -j u [\rho E_T + p] / r \quad (6)$$

$$\text{Species: } \partial_t \rho Y_k + \partial_r \rho u Y_k = -j \rho Y_k u / r \quad (k=1,2) \quad (7)$$

where  $\rho$  represents density,  $u$  is radial velocity,  $p$  denotes thermodynamic pressure,  $E_T$  is the total energy

**Table 1.** Fitting constants for  $E(T)$  for Equation (1).

$i$	$\rho/\rho_0$	$a_i$	$b_i$	$\alpha_i$
1	10	0.798	0.106	2.37
2	1	0.623	0.128	2.30
3	0.1	0.0595	0.246	1.98

**Figure 2.** Locus of states of air in the Le Chatelier plane of specific internal energy versus temperature (Gilmore, 1955).**Figure 3.** Equilibrium composition of dry air: nitrogen and oxygen molecules, atoms and ions at strong shock conditions (Gilmore, 1955).

$(E_T \equiv E + 0.5\rho\mathbf{u} \cdot \mathbf{u})$  with  $E$  being the thermodynamic energy, and  $Y_k$  represents the component mass fraction:  $k=1$  denotes DP gases and  $k=2$  denotes air, obeying the conservation relation:  $Y_{DP} + Y_A = 1$ . Here  $j$  denotes the geometry factor  $j \equiv d\ln A/d\ln r$  that equals 0, 1 or 2 for plane-, line-, or point-symmetric flows; see Oczarek [15] for more details.

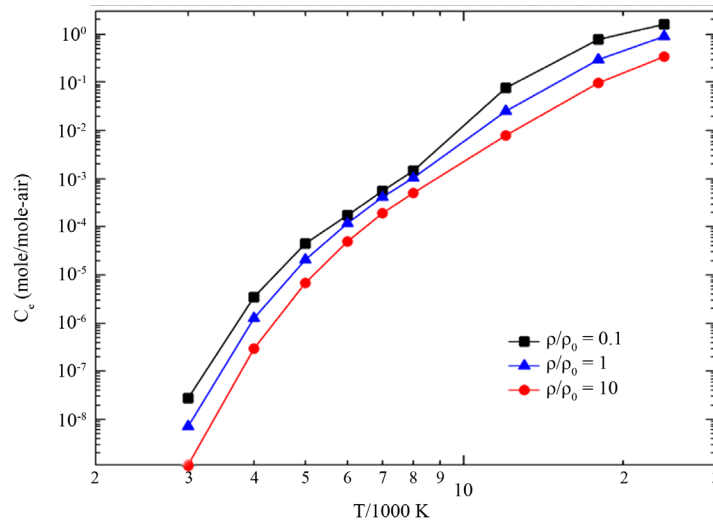


**Figure 4.** Electron concentrations in dry air (Gilmore 1955).

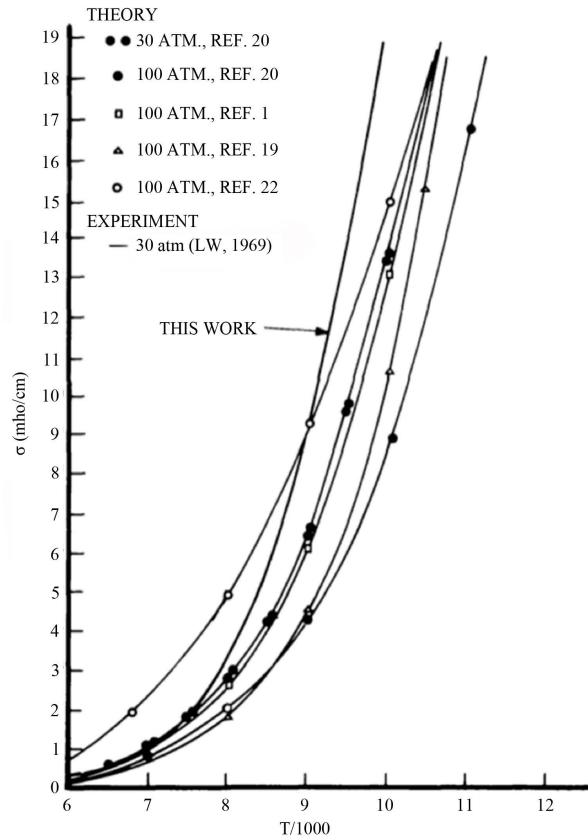


**Figure 5.** Electrical conductivity of air as measured by Larson & Williams (1969); Figure references are: Ref. 1: W. E. Nicolet *et al.* (1975) *Analytical and Design Study for a High-Pressure, High-Enthalpy Constricted Arc Heater*, **AEDC-TR-75-47**. Ref. 19: I. A. Sokolova (1974) *Transport Coefficients of Air at Temperatures from 3000 to 25,000 K, and Pressures of 0.1, 1, 10 and 100 Atm.*, **AD-779-809**. Ref. 20: R. W. Libermann (1976) Westinghouse Research Laboratories (private communication). Ref. [22]: T. C. Peng and A. L. Pindroh (1961) "An Improved Calculation of Gas Properties of High Temperature Air, paper 1995-61, 4<sup>th</sup> Biennial Gas dynamics Symposium, American Rocket Society.

### 3.2. Equations of State

The above system is closed by equations of state (EOS), which specify pressure in terms of internal energy and density. For pure air cells ( $Y_A = 1$ ), one evaluates the temperature by inverting Equation (1), yielding:

$$\log T = \left[ \log(E - E_0) - a_i \right] / b_i^{1/\alpha_i} \quad (8)$$

The pressure is then evaluated from the perfect gas law:

$$p_A = \rho RT \quad (9)$$

For pure DP cells ( $Y_{DP} = 1$ ), the loci of states are specified along the CJ isentrope in the Le Chatelier plane [16] [17]. They are fit by quadratic functions  $E(T) = aT^2 + bT + c$ , which may be inverted to evaluate temperature:

$$T = \left[ -b + \sqrt{b^2 - 4a(c - E)} \right] / 2a \quad (10)$$

The pressure is then evaluated from a perfect-gas form of the JWL function [17]:

$$p_{DP} = A \exp(-R_1 v) + B \exp(-R_2 v) + \rho RT \quad (11)$$

where  $v = \rho_0 / \rho$  and the constants are  $A = 1328$  GPa,  $B = 33.57$  GPa,  $R_1 = 6.321$  and  $R_2 = 2$  for TNT. For mixed cells one constructs a mixture curve in the Le Chatelier plane, based on the mass fractions  $Y_{DP}$ ,  $Y_A$  and then solves for the mixture temperature:  $T_m$ . This is used to calculate the partial pressures  $p_A$ ,  $p_{DP}$  from Equations (9) and (11); the mixture pressure:  $p_m$  is then calculated from the ideal gas relation:

$$p_m = p_A Y_A + p_{DP} Y_{DP} \quad (12)$$

### 3.3. Numerical Methods

The above system of partial differential Equations (4)-(7) is hyperbolic; it was integrated by the original high-order Godunov scheme developed by Colella and Woodward [18], based on a Riemann solver for real gases including detonation products by Colella and Glaz [19]. We assume that energy is released in the charge by a constant-velocity detonation wave starting at the origin ( $r = 0$ ). We model the flow field behind the detonation front by the similarity solution for a spherical Chapman-Jouguet (CJ) detonation wave, depicted in Figure 6 [20]. A 1-kg spherical TNT charge with a density of  $\rho_0 = 1.65$  g/cc was assumed. A uniform grid with an extremely fine mesh ( $\Delta r = 10 \mu\text{m}$ ) was used. The similarity solution was mapped onto the computational grid when the detonation wave reached the charge radius  $r_c = 5.27$  cm, forming an initial-value problem.

## 4. Blast Wave from a Spherical TNT Charge

The blast wave generated by the detonation of a spherical TNT charge was first calculated by Hal Brode in 1957 [21]; he used a one-dimensional (1D) Lagrangian gas-dynamic code, based on a Leapfrog scheme employing a Von Neumann artificial viscosity. Brode's manuscript provides a comprehensive description of the blast wave fields, from their inception to their decay into an acoustic wave. However, it gives no information on conductivity and EM effects studied here.

We simulate the same problem using the Eulerian gas-dynamic model, integrated by the non-diffusive high-order Godunov scheme, devoid of artificial viscosity. Of special focus in the present simulation is the formation of the conductive shock-heated air layer as the DP gases begin to expand. The EOS model (8)-(9) was used to accurately model the thermodynamic properties of air up to 24,000 K. Also, an extremely-fine mesh ( $\Delta r = 10 \mu\text{m}$ ) was used to capture the wave structure at shock breakout.

The blast wave formed from the detonation of the 1-kg TNT charge is presented in Figure 7. The wave structure of pressure, density, temperature and radial velocity are depicted in Figures 7(a)-(d); the profiles are qualitatively similar to Brode's solution (for more details on the flow field, consult figures 6-30 of his report). Of special interest here are the conductivity and specific current waves presented in Figure 6(e), Figure 6(f). Just after breakout, the conductivity wave peaks at 17 mho/cm and decays thereafter.

The blast wave flow field at  $t = 2.5 \mu\text{s}$  is depicted in Figure 8. A magnified view of the shock-heated air shell is shown in Figure 9. Mesh convergence studies indicated that the specific current profiles were converged

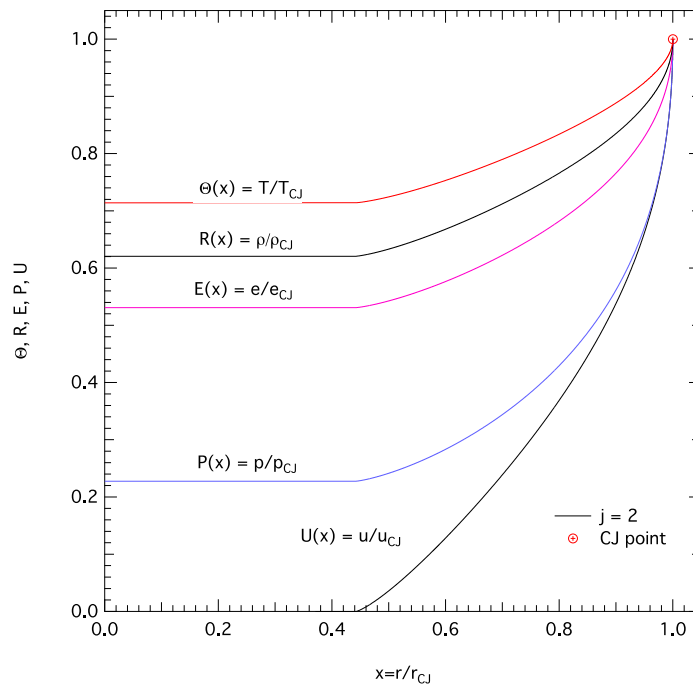


**Figure 6.** Similarity solution for a spherical ( $j = 2$ ) Chapman-Jouguet (CJ) detonation wave in TNT. CJ values listed in [Table 2](#).

**Table 2.** The CJ State<sup>\*</sup>

Variable	State
$p_{CJ}$ (bar)	197.6
$\rho_{CJ}$ (g/cc)	2.162
$T_{CJ}$ (K)	3237
$e_{CJ}$ (cal/g)	1404.8
$S_{CJ}$ (cal/g-K)	1.585
$u_{CJ}$ (km/s)	1.686
$W_{CJ}$ (km/s)	7.179

<sup>\*</sup> $\rho_0 = 1.654$  g/cc.

with a mesh spacing of  $\Delta r = 10 \mu\text{m}$ . One can recognize the mesh size since the symbols indicate the cell values. The width of the shock-heated air layer is  $\sim 1$  mm at this time, and contains  $\sim 100$  computational cells. The air temperature peaks at about 10,000 K. This creates significant ionization: with electron concentrations of  $\sim 10^{24}$  particles/m<sup>3</sup>, conductivity of  $\sim 17$  mho/cm, and specific current<sup>3</sup> of  $\sim 9$  mho/ $\mu\text{s}$ .

The species profiles in the blast wave at  $t = 2.5 \mu\text{s}$  are presented in [Figure 10\(a\)](#). A blowup of the shock-heated air region is shown in [Figure 10\(b\)](#). The air species peak at  $r = 6.89$  cm; peak values are listed in [Table 3](#). One sees that the electron concentrations peak at about 2.2 mole% in the air shell at this time. Ionization of nitric oxide forming  $\text{NO}^+$  is the primary electron source. It is worth recalling that prediction of this electron concentration is based solely on interpolation from Gilmore's table 10 summarizing the equilibrium solution of the thermodynamic system of dry air. The species profiles of the detonation products are depicted in [Figure 10\(a\)](#); peak values are listed in [Table 3](#). The detonation products are dominated by carbon solid (graphite) at 19 moles; the remaining major species are water vapor (8.3 moles), carbon dioxide (6.5 moles), diatomic nitrogen (4.6 moles) and carbon monoxide (1.47 moles). The electron concentration reaches  $\sim 0.17$  mole %—or about

<sup>3</sup>Here we define “specific current” as Ohm's current per unit magnetic field strength:  $\sigma u_r = J_\theta / B_0$ .



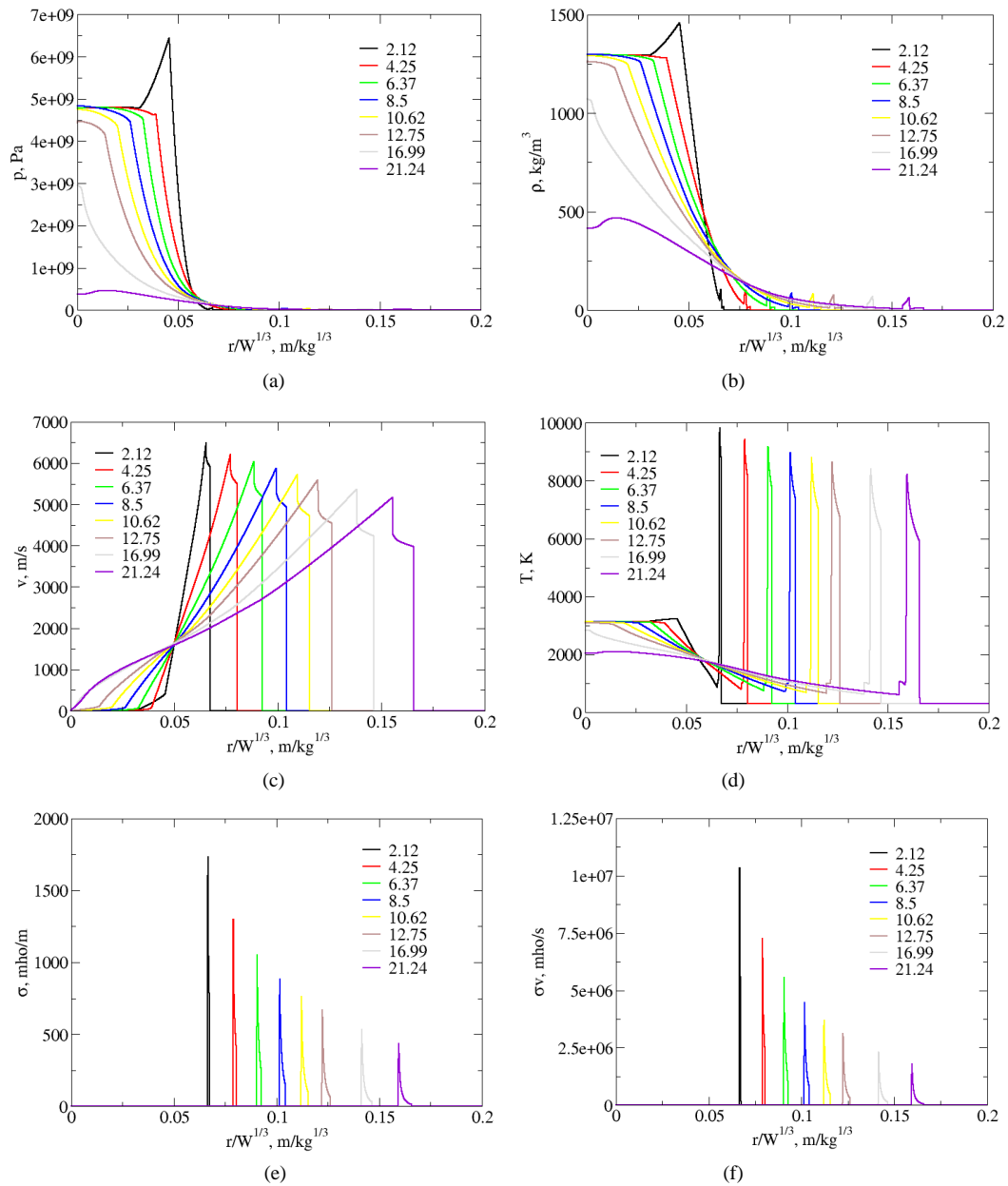


**Figure 7.** Evolution of the blast wave field created by the detonation of a 1-kg spherical TNT charge. (a) pressure; (b) density; (c) radial velocity; (d) temperature; (e) conductivity; (f) specific current.

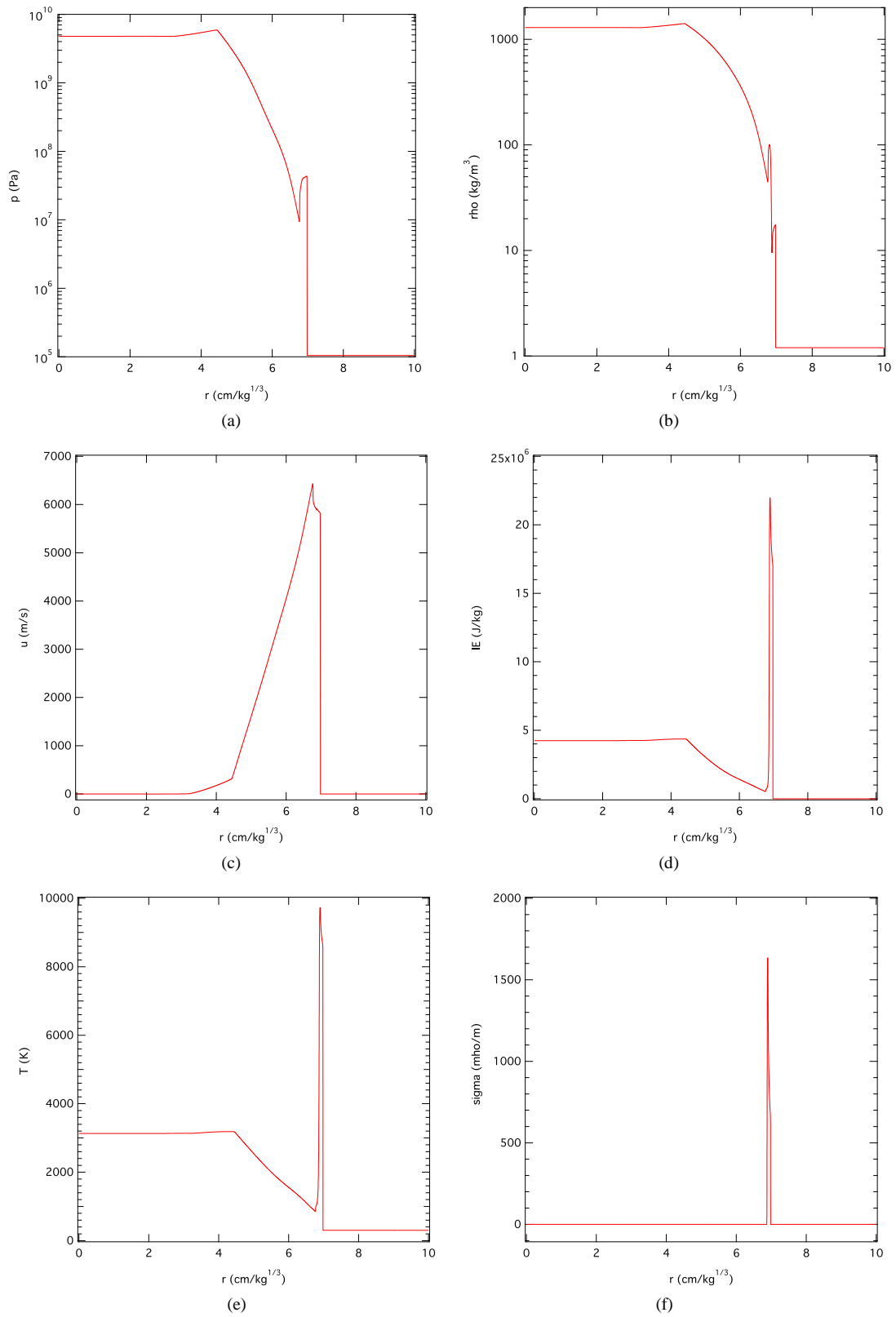
10% of that found in the air shell. The atom and molecular concentration values are based solely on interpolations of the thermodynamic equilibrium solution for the detonation products system at this state, as predicted by the Cheetah code [22]. Cheetah does not contain ionic physics at this state, so electron concentrations were evaluated by a quantum-mechanical formula for carbon graphite, as published by Ershov [23]; his model depends on the local temperature and graphite concentration.

## 5. EM Emissions from the Blast Wave

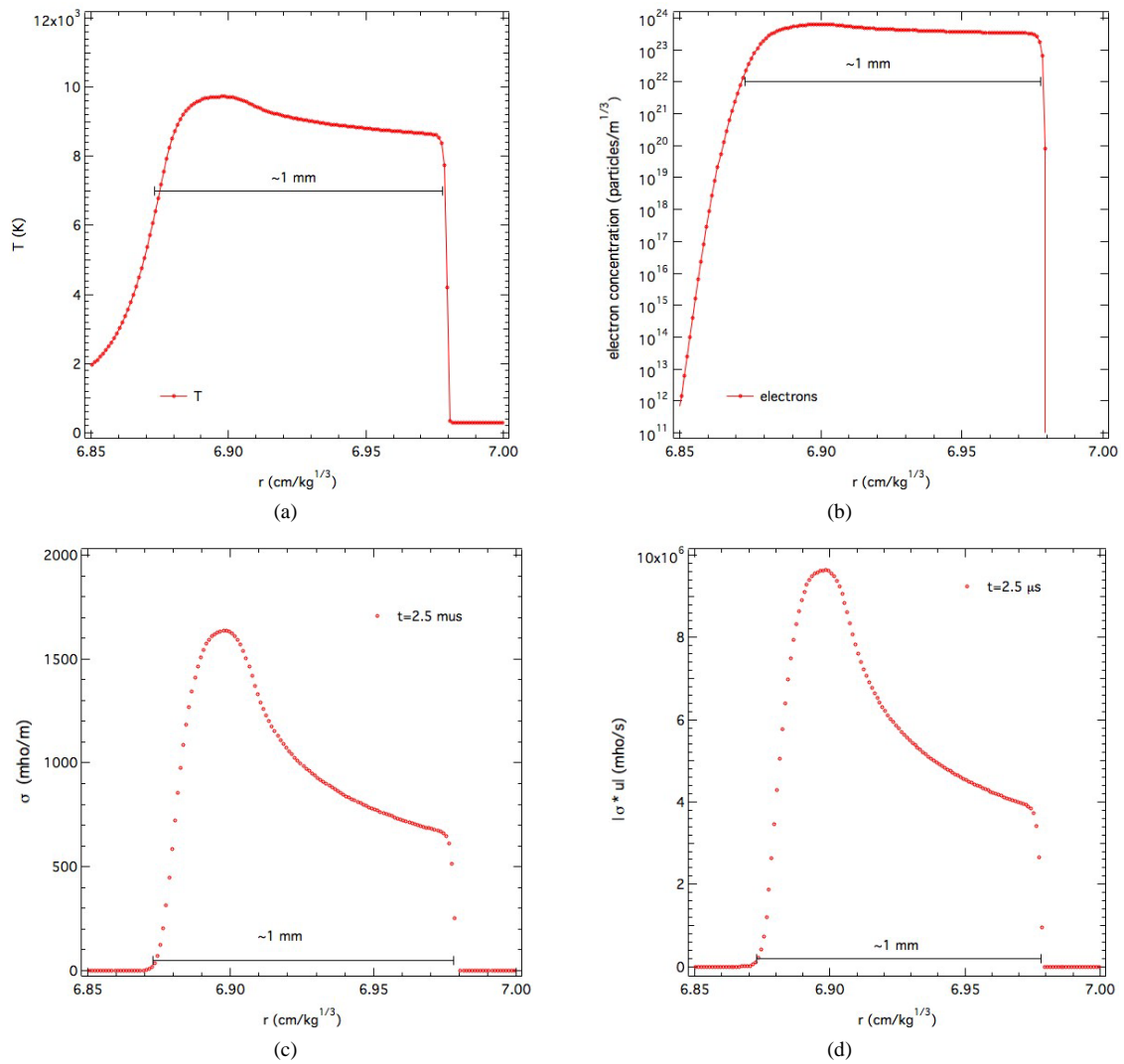
### 5.1. Boronin Current

The decay of the peak specific current created by TNT blast waves is shown in **Figure 11**. Two cases are considered: 1) self-similar Chapmann-Jouguet (CJ) detonation wave, and 2) Constant Volume Detonation (CVD) im-

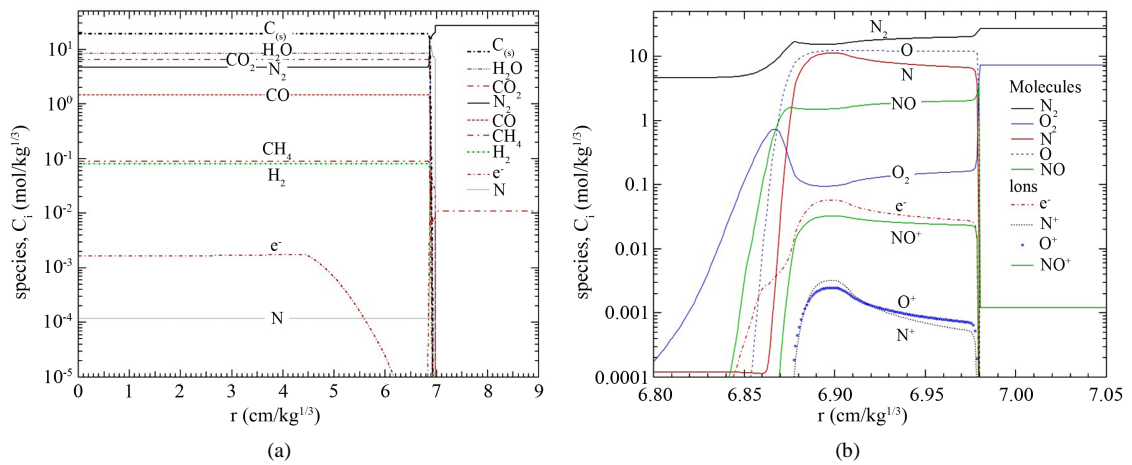




**Figure 8.** Blast wave flow field from 1-kg TNT explosion at  $2.5 \mu\text{s}$ . (a) pressure; (b) density; (c) radial velocity; (d) internal energy; (e) temperature; (f) conductivity.



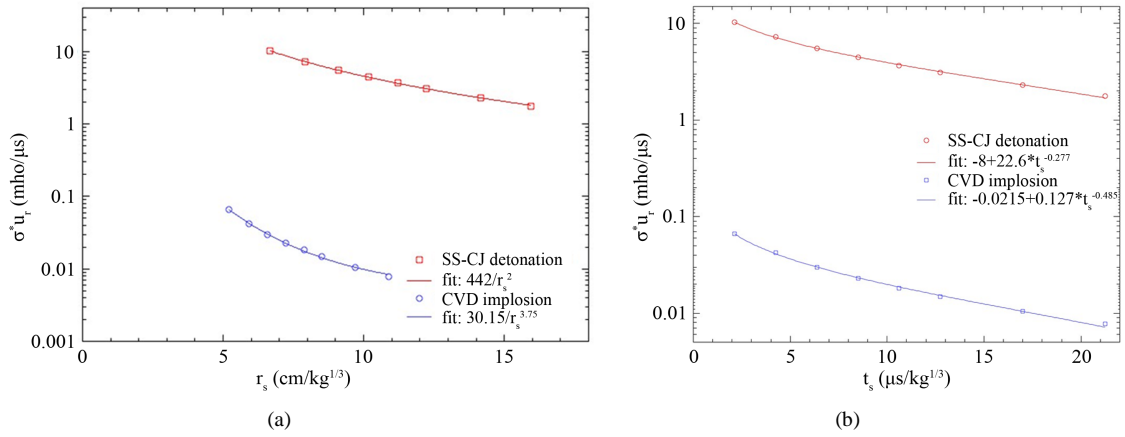
**Figure 9.** Structure of the shock-heated air shell at  $2.5 \mu\text{s}$ . (a) temperature; (b) electron concentration; (c) conductivity; (d) specific current.



**Figure 10.** Species profiles in a blast wave from a 1 kg spherical TNT charge at  $2.5 \mu\text{s}$ . (a) Over-all flow field; (b) blowup in shock-heated air region.

**Table 3.** Species Composition at  $t = 2.5 \mu\text{s}$ .

Shock-heated air		Detonation products	
Species	$C_i$ (mol/kg <sup>1/3</sup> )	Species	$C_i$ (mol/kg <sup>1/3</sup> )
N <sub>2</sub>	16.5	C <sub>(s)</sub>	19.1
O	9.2	H <sub>2</sub> O	8.3
N	5.3	CO <sub>2</sub>	6.5
NO	1.5	N <sub>2</sub>	4.6
O <sub>2</sub>	0.12	CO	1.47
e <sup>-</sup>	0.02235	e <sup>-</sup>	0.001666
NO <sup>+</sup>	0.0184	CH <sub>4</sub>	0.088
O <sup>+</sup>	0.0006	H <sub>2</sub>	0.081
N <sup>+</sup>	0.00047	N	0.0001

**Figure 11.** Decay of peak specific current for blast waves created by a self-similar CJ detonation versus a CVD implosion for 1-kg spherical TNT charges; (a) decay with range; (b) decay with time.

plosion wave. The implosion case produces currents that are approximately two orders of magnitude smaller than the CJ detonation wave, because it drives a much weaker air shock. The peak specific current decays as  $1/r^2$  for the CJ detonation case and  $1/r^4$  for the implosion case. The peak specific current decays in time as  $1/t^{0.3}$  for the CJ detonation case and as  $1/t^{0.5}$  for the implosion case.

This creates a “Boronin current” whose geometry is shown in **Figure 12**. According to Ohm’s Law<sup>4</sup>:

$$\mathbf{J}_\theta = \sigma \mathbf{u}_r \times \mathbf{B}_0 \quad (13)$$

An azimuthal current:  $\mathbf{J}_\theta$  is generated in the shock-heated conductive air shell by the vector-cross-product of the radial velocity  $\mathbf{u}_r$  and the earth’s magnetic field:  $\mathbf{B}_0 = 0.5 \text{ Gauss} \cdot \mathbf{i}_y$ . Using the fits from **Figure 11**, this takes the form:

$$\mathbf{J}_\theta(a, \phi, t) = c \mathbf{B}_0 \sin \phi / t_s^{0.277} \quad (14)$$

$$\mathbf{J}_\theta(a, \phi, t) = -0.277 c \mathbf{B}_0 \sin \phi / t_s^{1.277} \quad (15)$$

where  $a$  denotes the radius of the peak specific current:  $\phi$  the angle of declination from the  $z$  axis, and  $c = 22.6$ . A three-dimensional visualization of the Boronin current is depicted in **Figure 12**.

This azimuthal current:  $\mathbf{J}_\theta$  induces a magnetic field  $\mathbf{B}$ , according to the Biot-Savart Law:

<sup>4</sup>We start from the generalized Ohm’s Law:  $\mathbf{J} = \sigma(\mathbf{E} + \mathbf{u} \times \mathbf{B})$  where all vectors are in lab-fixed coordinates. For the present case, initial conditions are:  $\mathbf{E} = \mathbf{E}_0 = 0$  and  $\mathbf{B} = \mathbf{B}_0 = (0.5 \text{ gauss}) \mathbf{i}_y$ .

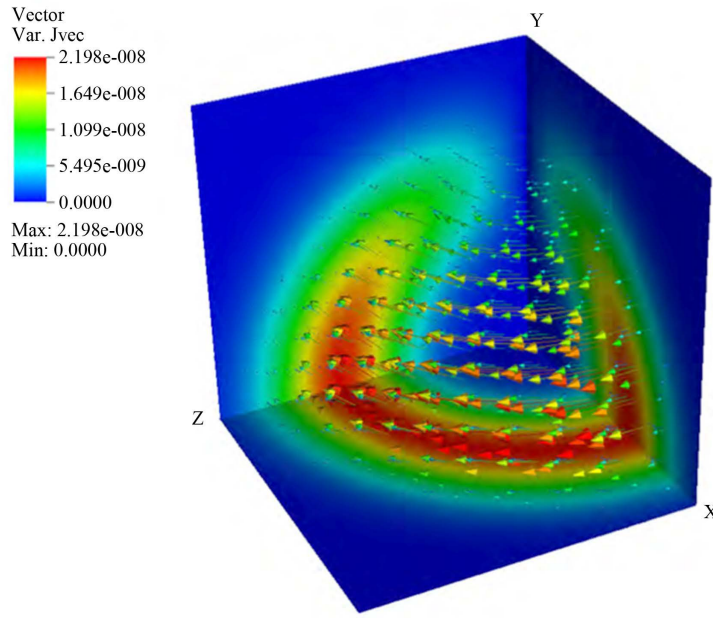


**Figure 12.** Visualization of the Boronin current in the shock-heated air shell. The current rotates about the Earth's magnetic field vector  $\mathbf{B}_0$ , which is aligned with the  $y$ -axis. The current is maximum in the  $z$ - $x$  plane of  $y = 0$ , and decays to 0 on the  $y$ -axis, according to the  $\sin\phi$  dependence of the vector-cross-product of Equation (13).

$$\mathbf{B}(\mathbf{x}, t) = \frac{\mu_0}{4\pi} \iiint \mathbf{J}_\theta(\mathbf{r}, t) \times \frac{\mathbf{x} - \mathbf{x}'}{|\mathbf{x} - \mathbf{x}'|^3} d^3x' \quad (16)$$

As an approximation, assume that the current is concentrated on the equator (e.g., as a conducting wire at radius  $r = a$  of conductivity  $\sigma$ ); then one can find an approximate analytic solution to the integral of (16):

$$B_r(r, \phi, t) = \frac{\mu_0}{2\pi} [J_\theta(a, t) \pi a^2] \cos\phi / r^3 \quad (17)$$

$$B_\phi(r, \phi, t) = \frac{\mu_0}{2\pi} [J_\theta(a, t) \pi a^2] \sin\phi / r^3 \quad (18)$$

as derived by Jackson [24]. This shows that the field decays as  $1/r^3$ .

## 5.2. Electromagnetic Waves

The above represents an approximate magneto-static solution. However, we are interested in the wave solution. The time-domain Green's function approach [11] can be used to predict electric and magnetic waves in space and time. The Green's function takes the form:

$$\mathbf{G} = -\frac{\delta'(\tau - R/c)}{4\pi\epsilon R} \mathbf{I} + \nabla \nabla \frac{U(\tau - R/c)}{4\pi\epsilon R} \quad (19)$$

where  $U$  is the Heaviside function,  $\delta'$  is the derivative of the Dirac delta function,  $R$  is the distance between observer and source:  $R = |\mathbf{x}_{\text{obs}} - \mathbf{x}_s|$  and  $\tau$  is retarded time:  $\tau = t_{\text{obs}} - t_s$ . The electric field strength is calculated from the integral:

$$\mathbf{E}(r_{\text{obs}}, t) = \int_0^t \int_V \mathbf{G} \cdot \mathbf{J}(r_s, t_s) d\mathbf{r}_s dt_s \quad (20)$$

One can think of this approach as a generalization of the Biot-Savart Law (16), to include causality effects in

time. Given  $\mathbf{E}$ , the magnetic field strength  $\mathbf{H}$  is then calculated from the integral of Faraday's Law:

$$\mathbf{H} = -\frac{1}{\mu_0} \int \nabla \times \mathbf{E} dt \quad (21)$$

See White and Fassenfest [25] for more details.

With the analytic description of the Boronin current (Figure 11) as input, the above method predicts the electric and magnetic field waveforms at selected points of observation:  $r_{\text{obs}}$ . Results are presented in Figure 13 and Figure 14, which show the time history of the electric and magnetic fields at distances from 10 meters to 10 km from the HE explosion.

At close-in ranges ( $r = 10$  m), the waveforms are quite different. For example, the electric field vector  $E_y$  has a narrow waveform with negative phase of similar area to the positive phase; the magnetic vector  $H_z$  is about 100 times larger and had a single broad positive phase waveform. Arrival time at 10 meters was about  $10 \mu\text{s}$  and pulse duration was about  $20 \mu\text{s}$ . At 100 meters, the waveforms were qualitatively similar to their cousins at 10 meters, but had decayed significantly in magnitude. Arrival time and waveform duration were similar at 10 meters and 100 meters.

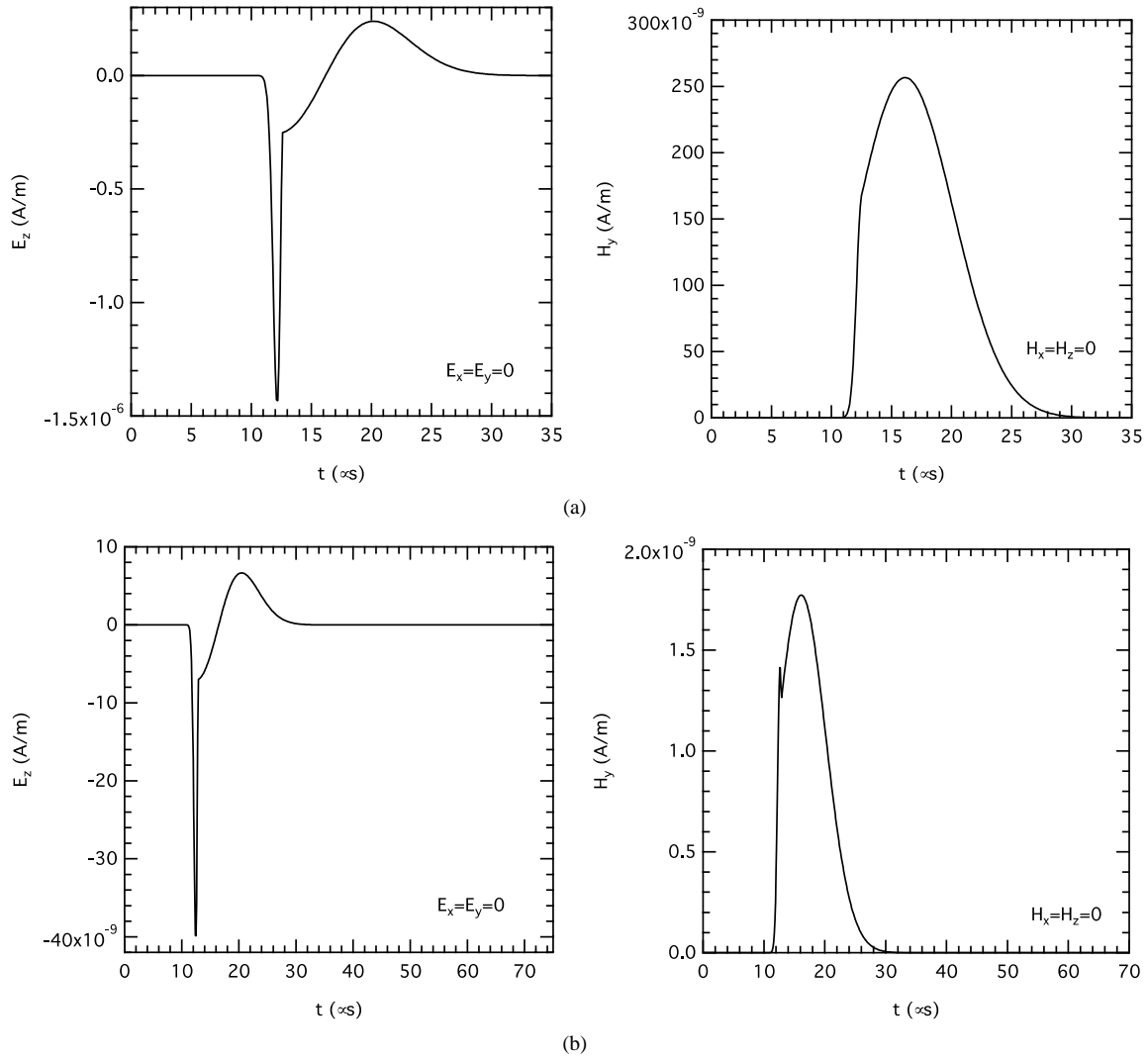


**Figure 13.** Predicted electric- and magnetic-field waveforms from a 1-kg TNT explosion in the near field. Note: the earth's magnetic field  $\mathbf{B}_0$  is aligned with the  $+y$ -axis; due to spherical symmetry of the source,  $E_x = E_y = 0$  and  $H_x = H_z = 0$ . (a) Solution at  $x = 10$  m; (b) Solution at  $x = 100$  m.

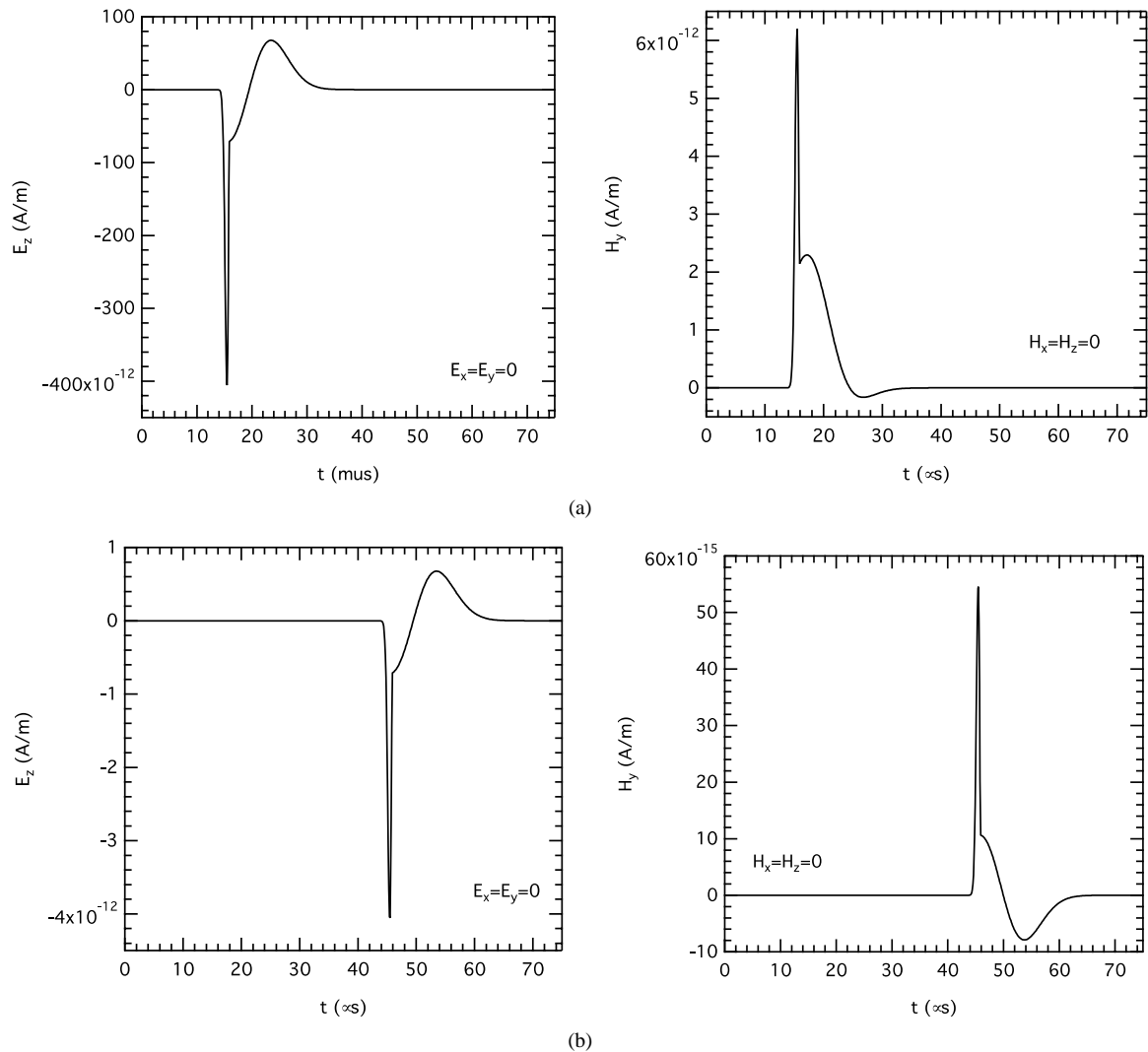


**Figure 14.** Predicted electric- and magnetic-field waveforms from a 1-kg TNT explosion in the far field. Note: the earth's magnetic field  $\mathbf{B}_0$  is aligned with the +y-axis; due to spherical symmetry of the source,  $E_x = E_y = 0$  and  $H_x = H_z = 0$ . (a) Solution at  $x = 1000$  m; (b) Solution at  $x = 10,000$  m.

Waveforms in the far field (1 km and 10 km) are presented in **Figure 14**. The electric field  $E_y$  histories have a positive and negative phase, similar to those at close-in ranges. The magnetic field  $H_z$  waveforms have changed, and now contain a negative phase similar to the electric field histories, because they asymptotically approach plane waves. Arrival of EM waves at 1 and 10 km were about 15 and 45  $\mu\text{s}$ , respectively. Pulse duration was still about 20  $\mu\text{s}$  (corresponding to the current duration shown in **Figure 7(f)**).

## 6. Discussion

The Green's function solution shows conclusively that the Boronin current will generate electromagnetic waves that can propagate to large distances. Magnitudes of these waves are small, e.g.,  $\sim 10^{-6}$  A/m at 10 meters, and decay to between  $10^{-12}$  to  $10^{-14}$  A/m at 10 kilometers. No doubt they are small because they are proportional to the earth's magnetic field  $\mathbf{B}_0$ , which is small.

Potentially, there are other sources of EM emissions in explosions. For example, detonation waves in many CHNO explosives (TNT, dntf, C4, Comp B, TATP) produce large amounts of Carbon graphite. Measurements indicate that the Carbon graphite is conductive [23], and will produce an "Ershov current" [26] in the detonation

products, similar to the Boronin current in shock-heated air—thereby generating EM waves from the detonation itself. This may indeed be the source of EM waves measured by Kolsky in 1954. It is also known that there is ionization in flame sheets embedded in the turbulent combustion field in TNT fireballs [8]–[10]; see **Figure 1** for an example. One expects that the movement of such ionization patches by the turbulent velocity field can generate electric “combustion currents”—leading to random EM emissions (noise) from the fireball, which can last for durations ( $\sim 50 \text{ ms/kg}^{1/3}$ ) much longer than the Boronin effect ( $\sim 20 \text{ }\mu\text{s/kg}^{1/3}$ ). And there are other potential effects such as tribo-electric discharges, electron-transfer reactions, etc. But these are beyond the scope of the present work, and will be explored in future publications.

## 7. Conclusion

According to Kolsky and others, electromagnetic waves are emitted when HE charges are detonated. Boronin proposed that they are related to “an ionized air layer on the shock front”. We have illustrated the *Boronin mechanism* for spherical charges of TNT via numerical simulations. Applying Ohm’s Law, we show that this expanding ionization wave will create an azimuthal current, and the time-domain Green’s function method predicts electromagnetic wave radiation. For an unconfined explosion with no ground reflections, the duration of this source is estimated to be  $\sim 20 \text{ }\mu\text{s/kg}^{1/3}$  (i.e., the time when the shock-heated air shell cools below 2000 K needed to ionize the air). Being proportional to the earth’s magnetic field  $B_0$ , the computed EM waves are rather weak (e.g.,  $10^{-4}$  to  $10^{-6}$  A/m at 10 meters). To accurately predict the Boronin current, one needs an extremely fine-zoned grid ( $\Delta r = 10 \text{ }\mu\text{m/kg}^{1/3}$ ) for the gasdynamics, an accurate description of the thermodynamic properties of high-temperature air, and an accurate model of the electrical conductivity of air.

## Acknowledgements

This work performed under the auspices of the US Department of Energy by Lawrence Livermore National Laboratory under Contract DE-AC52-07NA27344. **LLNL-JRNL-655186**.

## References

- [1] Kolsky, H. (1954) Electromagnetic Waves Emitted on Detonation of Explosives. *Nature*, **173**, 77. <http://dx.doi.org/10.1038/173077a0>
- [2] Takakura, T. (1955) Radio Noise Radiated on the Detonation of Explosives. *Publications of the Astronomical Society of Japan*, **7**, 210–220.
- [3] Cook, M.A. (1958) The Science of High Explosives. Reinhold Publishing, New York, 440 pp. (*vid. esp.* Chapter 7: Ionization, Electrical, Magnetic and Electromagnetic Phenomena Accompanying Detonation).
- [4] Boronin, A.P., Kapinos, V.N., Krenev, S.A. and Mineev, V.N. (1990) Physical Mechanism of Electromagnetic Field Generation during the Explosion of Condensed Explosive Charges: Survey of Literature. *Combustion Explosion & Shock Waves*, **26**, 597–602. <http://dx.doi.org/10.1007/BF00843137>
- [5] Adushkin, V.V. and Soloviev, S.P. (2004) Generation of Electric and Magnetic Fields by Air, Surface and Underground Explosions. *Combustion Explosion & Shock Waves*, **40**, 649–657. <http://dx.doi.org/10.1023/B:CESW.0000048266.03133.51>
- [6] Kuhl, A.L. (2010) Conductivity Histories Measured in Shock-Dispersed-Fuel Explosion Clouds. Lawrence Livermore National Laboratory Report **LLNL-TR-427483**, 18 pp.
- [7] Kuhl, A.L. and Bell, J.B. (2011) Adaptive High-Resolution Methods for Simulating Combustion in Explosions, 42<sup>nd</sup> Int. Annual Conference of ICT: *Energetic Materials*, Fraunhofer-Institut für Chemische Technologie, Postfach, 26-1 to 26-16.
- [8] Kuhl, A.L., Bell, J.B., Beckner, V.E. and Reichenbach, H. (2010) Gasdynamic Model of Turbulent Combustion in TNT Explosions. *Proceedings of the Combustion Institute*, **33**, 2177–2185.
- [9] Kuhl, A.L., Bell, J.B. and Beckner, V.E. (2010) Heterogeneous Continuum Model of Aluminum Particle Combustion in Explosions. *Combustion Explosion & Shock Waves*, **46**, 433–448. <http://dx.doi.org/10.1007/s10573-010-0058-9>
- [10] Kuhl, A.K., Bell, J.B., Beckner, V.E., Balakrishnan, K. and Aspden, A.J. (2013) Spherical Combustion Clouds in Explosions. *Shock Waves*, **23**, 233–249. <http://dx.doi.org/10.1007/s00193-012-0410-y>
- [11] Nevels, R. and Jeong, J. (2004) The Time-Domain Green’s Function and Propagator for Maxwell’s Equations. *IEEE Transactions on Antennas and Propagation*, **52**, 3012–3018. <http://dx.doi.org/10.1109/TAP.2004.835123>
- [12] Gilmore, F.R. (1955) Equilibrium Composition and Thermodynamic Properties of Air to 24,000 K, Rand Corp. Report



- RM-1543**, 68 pp;  
also see DASA 1971-1 *THERMAL RADIATION PHENOMENA*, In: Magee, J.L. and Aroeste, H., Eds. (1967) 3-27-67-1 Vol. 1, 333 pp. (*vid. esp.* Chapter 1: The Equilibrium Thermodynamic Properties of High Temperature Air by F. R. Gilmore;
- [13] Glueckauf, E. (1951) The Composition of Atmospheric Air. In: Malone, T.F., Ed., *Compendium of Meteorology*, American Meteorological Society, Boston.
  - [14] Larson, A.V. and Williams, R.J. (1977) Electrical and Thermal Conductivity and Radiation Power of Air Measured AT 1-30 ATM and 6,500-11,500°K. AEDC-TR-77-69, 54 p.
  - [15] Owczarek, J.A. (1964) Fundamentals of Gas Dynamics. International Textbook Company, Scranton, 273-277.
  - [16] Kuhl, A.L. and Khasainov, B. (2007) Quadratic Model of Thermodynamic States in SDF Explosions. *38th International Annual Conference of the Institut Chimische Technologie on Energetic Materials*, 143.1-143.11.
  - [17] Kuhl, A.L. (2006) Thermodynamics of Combustion of TNT Products in a Chamber. *Combustion, Explosion and Shock Waves*, **25**, 42-48.
  - [18] Colella, P. and Woodward, P. (1984) The Piecewise-Parabolic Method (PPM) for Gas-Dynamical Simulations. *Journal of Computational Physics*, **54**, 174-201. [http://dx.doi.org/10.1016/0021-9991\(84\)90143-8](http://dx.doi.org/10.1016/0021-9991(84)90143-8)
  - [19] Colella, P. and Glaz, H. (1985) Efficient Solution Algorithms for the Riemann Problem for Real Gases. *Journal of Computational Physics*, **59**, 264-289. [http://dx.doi.org/10.1016/0021-9991\(85\)90146-9](http://dx.doi.org/10.1016/0021-9991(85)90146-9)
  - [20] Kuhl, A.L., Balakrishnan, K., Bell, J.B. and Beckner, V.E. (2014) On the Structure of Self-Similar Detonation Waves in TNT Charges. *35th International Combustion Symposium*, in press.
  - [21] Brode, H.L. (1959) Blast Wave from a Spherical Charge, *Physics of Fluids*, **2**, 217-229;  
also see Brode, H.L. (1957) Calculation of the Blast Wave from a Spherical Charge of TNT, Rand Corp. **RM-1965**, 1-68 (*vid. esp.* Figure 29).
  - [22] Fried, L.E. (1995) CHEETAH 1.22 User's Manual. LLNL, UCRL-MA-117541.
  - [23] Ershov, A.P. (1975) Ionization during the Detonation of Solid Explosives. *Fizika Goreniyai Vzryva*, **11**, 798-803.
  - [24] Jackson, J.D. (1962) Classical Electrodynamics. 2nd Edition, John Wiley, New York (*vis. esp.* Equation (5.41)).
  - [25] White, D. and Fasenfest, B. (2014) Electromagnetic Emissions from Explosives: Magnetic Bubble Effect. Lawrence Livermore National Laboratory, LLNL-TR-655184, 34 p.
  - [26] Kuhl, A.L. (2014) Model of Conductivity Profiles in TNT Detonations. *35th Detonation Symposium*, in press.

Scientific Research Publishing (SCIRP) is one of the largest Open Access journal publishers. It is currently publishing more than 200 open access, online, peer-reviewed journals covering a wide range of academic disciplines. SCIRP serves the worldwide academic communities and contributes to the progress and application of science with its publication.

Other selected journals from SCIRP are listed as below. Submit your manuscript to us via either [submit@scirp.org](mailto:submit@scirp.org) or [Online Submission Portal](#).

